Stacking-dependent deep level emission in boron nitride

A. Rousseau, P. Valvin, C. Elias, L. Xue, J. Li, J. H. Edgar, B. Gil, and G. Cassabois

Phys. Rev. Materials **6**, 094009 — Published 20 September 2022

DOI: 10.1103/PhysRevMaterials.6.094009

Stacking-dependent deep level emission in boron nitride

A. Rousseau,[1] P. Valvin,[1] C. Elias,[1] L. Xue,[2] J. Li,[2] J. H. Edgar,[2] B. Gil,[1] G. Cassabois[1,*]
[1] *Laboratoire Charles Coulomb UMR 5221 CNRS-Université de Montpellier, 34095 Montpellier, France*
[2] *Tim Taylor Department of Chemical Engineering, Kansas State University, Manhattan Kansas 66506, USA*
(Dated: September 12, 2022)

We report hyperspectral microscopy in sp^2-bonded boron nitride polytypes with a simultaneous inspection of the photoluminescence signal in the UV-C and UV-B spectral ranges. By comparing two different polytypes extracted from the same polycrystalline sample, we reveal that the well-known "4 eV defect" does not emit at the same energy for polytypes in the AB and AA' stackings. The zero-phonon line is either at 4.14 or 4.16 eV for the noncentrosymmetric AB stacking, instead of the usual 4.09 eV energy in the AA' stacking. Our results open the way for novel characterization methods of the stacking order in sp^2-bonded boron nitride, and bring novel inputs for the elucidation of the atomistic configuration of points defects by advanced *ab initio* calculations.

I. INTRODUCTION

Boron nitride is a compound semiconductor with a wide bandgap in the ultraviolet spectral range. Cubic boron nitride (cBN) is the most stable polymorph with sp^3-hybridization of the electronic states. Its hardness is comparable to diamond, and its thermal conductivity and its ∼10 eV-bandgap [1] make it a promising material in the expanding field of ultrawide bandgap semiconductors [2]. In contrast, hexagonal boron nitride (hBN) is made of honeycomb atomic planes with sp^2-hybridized bonds, the vertical stacking of which relies on weak van der Waals interactions. hBN corresponds to the so-called AA' stacking of atomic planes, where boron and nitrogen atoms alternate along the c-axis [3]. This is the most common sp^2-bonded boron nitride polytype. Since the first synthesis of large hBN single crystals by Watanabe *et al.* in 2004 [4], hBN has become a pivotal crystal in 2D materials research [5], and potentially providing a solution for optoelectronics in the UV-C range [6–8] thanks to its ∼6 eV-bandgap [9, 10].

There is a large variety of sp^2-bonded boron nitride polytypes [11]. Besides the most thermodynamically stable AA' phase of hBN and the many disordered phases of turbostratic boron nitride (tBN), several high-symmetry stacking orders are possible with close cohesive energies [11]. However, the macroscopic shapes of these polytypes do not change in contrast to the case of polymorphs, thus making their characterization and identification difficult. In a recent paper [12], Bernal boron nitride (bBN) crystals with AB stacking were identified by means of cryomicroscopy in the UV-C demonstrating a one-to-one correlation between inversion symmetry breaking probed by second harmonic generation and the detection of an intense photoluminescence (PL) line at ∼6.035 eV (λ∼205 nm), the specific signature of the noncentrosymmetric Bernal stacking. In the absence of any clear and easily accessible fingerprint either by optical microscopy, Raman spectroscopy, or X-ray diffraction [12, 13], relying on low-temperature experiments in the UV-C remains very demanding for studying polytypism in boron nitride. This issue hinders the exploration of the many polytypes of boron nitride, and the control of their growth, in the perspective of tuning their electronic and optical properties for boron nitride-based devices, in analogy to silicon carbide polytypes.

In this paper, we report hyperspectral microscopy in bBN and hBN crystals with a simultaneous inspection of the PL signal in the UV-C and UV-B spectral ranges. While the intrinsic optical response of bBN and hBN lies in the UV-C, at wavelengths between 200 and 215 nm close to the ∼6 eV band-edge, the emission of point defects features well-defined optical lines within the bandgap, in the UV-B around 300 nm. These correspond to the recombination of the well-known "4 eV defect", the origin of which is debated, and the subject of many experimental and theoretical studies [14–28]. By comparing bBN and hBN crystals extracted from the same polycrystalline sample, we reveal that the "4 eV defect" does not emit at the same energy for boron nitride polytypes in the AB and AA' stackings. In hBN the zero-phonon line (ZPL) is located at the canonical energy of 4.09 eV with a pronounced vibronic band [18]. In bBN there are two defect configurations with a ZPL at either 4.14 or 4.16 eV, together with a ZPL broadening. Our results open the way for characterizing the stacking order in sp^2-bonded boron nitride polytypes by means of optical spectroscopy in the UV-B, rather than in the highly-demanding UV-C spectral domain. Moreover, our study presents evidence of the stacking-dependent emission of deep levels in boron nitride, which could be useful for elucidating the atomistic configuration of points defects by advanced *ab initio* calculations.

II. OPTICAL RESPONSE IN THE UV-C

bBN is the noncentrosymmetric polytype of boron nitride that is isostructural to graphite. Both bBN and hBN have a bandgap in the range of ∼6 eV [9, 12, 13] but the different stackings slightly modify the electronic and optical properties [12, 13, 29–31]. The fundamental bandgap of bBN is indirect, as in hBN, but with a 75 meV-blueshift [12]. The main difference between

bBN and hBN is the quasi-degeneracy of indirect and direct excitons in bBN [12] while they are split by 170 meV in hBN [32]. This quasi-degeneracy is the signature of an unusually flat in-plane dispersion of the excitonic states for the AB stacking [29], that allows their simultaneous observation in luminescence experiments [12, 13]. As shown in Fig.1(a), there is an intense PL signal at ∼6.035 eV in bBN, that is the specific signature of the noncentrosymmetric Bernal stacking [12].

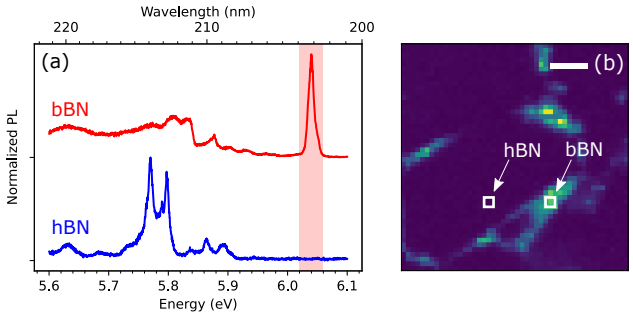

FIG. 1. (a) PL spectra in the UV-C, at 6 K, recorded for bBN (top, red line) and hBN (bottom, blue line) crystals, at the positions indicated by the white squares in (b). PL excitation energy = 6.39 eV. The bBN spectrum is vertically shifted for clarity. (b) Map of the PL signal around ∼6.035 eV (see shaded area in panel a). Scale bar = 4 μm.

The PL spectra in Fig.1(a) correspond to the typical optical response in the UV-C range of sp^2-bonded boron nitride polytypes extracted from a carbon-doped BN polycrystal precipitated from a metal solution, as described in Ref.[13, 23]. The fact that the crystals under study here are fabricated in exactly the same growth conditions is a key point for an accurate comparison of their optical response and the investigation of the only influence of the stacking sequence. PL mapping is performed in a scanning confocal cryomicroscope operating in the deep-ultraviolet, allowing hyperspectral imaging under above bandgap excitation at 6.39 eV [33, 34]. Fig.1(b) is a map of the PL signal integrated in a spectral window [shaded area in Fig.1(a)] centered at ∼6.035 eV, which is the specific energy of the direct recombination in bBN. Intense emission at this energy occurs in a micro-crystal in the AB stacking, inside which the top spectrum in Fig.1(a) [red line] is recorded, at the position indicated by the white square in Fig.1(b). We also note the marginal existence of an AB stacking at the edges of the large hBN crystal, which appears dark in Fig.1(b) and inside which the typical spectrum of the AA' stacking is measured [bottom blue line in Fig.1(a)], at the position indicated by the white square in Fig.1(b). Hyperspectral imaging being performed in the UV-C range in Fig.1, this first set of data essentially reproduces the previous results reported in Ref.[12, 13] where the identification of the AB stacking relies on the inspection of the emission around ∼6.035 eV (λ∼205 nm).

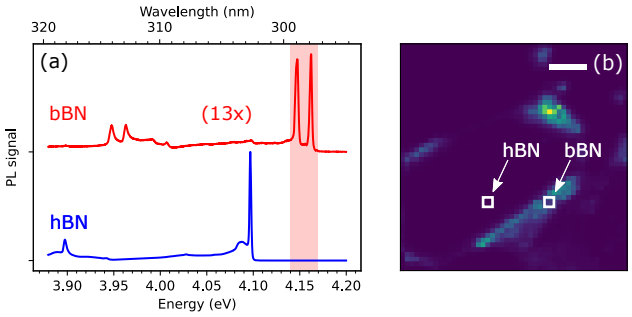

FIG. 2. (a) PL spectra in the UV-B, at 6 K, recorded for bBN (top, red line) and hBN (bottom, blue line) crystals, at the positions indicated by the white squares in (b). PL excitation energy = 6.39 eV. The bBN spectrum is vertically shifted for clarity. (b) Map of the PL signal around ∼4.15 eV (see shaded area in panel a). Scale bar = 4 μm.

III. OPTICAL RESPONSE IN THE UV-B

The complementary investigation of the UV-B range provides novel fingerprints for the AB stacking. In our hyperspectral imaging experiments, the diffraction grating of the spectrometer is rotated at each position of the sample in order to sequentially record the PL spectrum in the UV-C and UV-B ranges. Fig.2(b) is thus the map of the PL signal in the exact same region as for Fig.1(b). The spectral domain of integration is now in the UV-B range, around 300 nm [shaded area in Fig.2(a)] where the well-known "4 eV defect" emits [14–28].

In the hBN crystal, the PL spectrum features a sharp line at 4.09 eV, which is the ZPL of the defect, i.e. the direct recombination without any net energy transfer with the phonon bath. There is also PL emission at low energies due to phonon-assisted recombination in the defect. This vibronic band involves low-energy acoustic phonons for the emission at ∼4.08 eV close to the ZPL, zone-center optical phonons for the replica at 3.9 eV, and phonons spanning the full bandstructure as witnessed by the phonon-photon mapping in the vibronic band of this defect [18]. The PL spectrum recorded in the hBN crystal in Fig.2(a) [bottom blue line] is the canonical one reported in the literature [14–28]. **The corresponding PL map around 4.09 eV is plotted in Fig.4(a) in the Appendix.**

Surprisingly, the PL spectrum of the "4 eV defect" changes in the bBN crystal [top red line in Fig.2(a)]. In the micro-crystal in the AB stacking identified in Fig.1, the PL spectrum is globally blue-shifted and duplicated with two ZPLs at 4.14 or 4.16 eV [**see corresponding**

PL maps in Fig.4(b-c) in the Appendix]. The vibronic emission is globally unaffected but we notice a broadening of the ZPL from 2 meV in hBN to 4 meV in bBN. Because of this broadening it is difficult to conclude on a possible modification of the low-energy acoustic phonon sideband of the defect. Still, temperature-dependent measurements show that the thermal broadening of the ZPL is lower in bBN than in hBN [Fig.3]. **The dotted line in Fig.3 is a phenomenological fit of the ZPL broadening in hBN, following the standard expression:** $\Gamma(T) = \Gamma_0 + aT + be^{-\frac{\Delta}{k_B T}}$**, where** Γ_0 **is the zero-temperature limit of the linewidth,** aT **the acoustic-phonon broadening, and** $be^{-\frac{\Delta}{k_B T}}$ **the optical-phonon broadening, with** Γ_0**=1.9±0.2 meV,** a**=13±5** μ**eV.K**$^{-1}$**, and** b $\gtrsim$**20 meV, and** Δ $\gtrsim$**20 meV [18]. The quantitative interpretation of the ZPL broadening of the "4 eV defect" in bBN will require in-depth theoretical investigations, beyond the scope of this work.**

Although the ZPL shift is much larger than the ZPL broadening in Fig.2, thus making very clear the difference between the AA' and AB stackings, the ZPL shift does not follow the 75 meV blue-shift of the bandgap from hBN to bBN [12]. In bBN, the ZPL of the "4 eV defect" is blue-shifted by either 50 or 70 meV with respect to hBN, i.e. smaller values than the bandgap shift. Previous measurements demonstrated that these lines can be observed independently [23], thus ruling out that they correspond to different levels of a given microscopic structure but rather suggesting that the "4 eV defect" can exist in different atomistic configurations in the AB stacking of boron nitride.

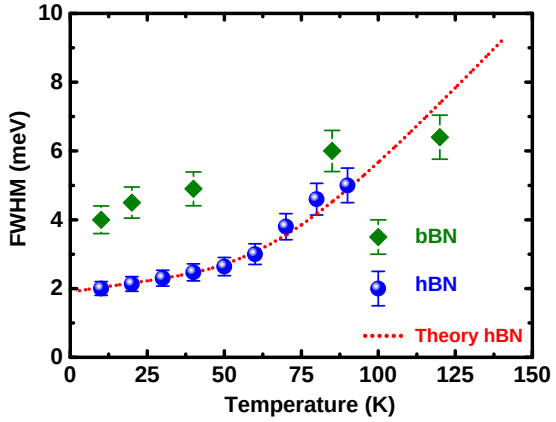

FIG. 3. Temperature dependence of the ZPL width in hBN (blue circles) and bBN (green diamonds). Dotted line : theoretical fit for hBN, from Ref.[18].

The PL spectra are spatially integrated in regions of the same area in Fig.2(b), so that the intensity of the ZPL allows a quantitative comparison of the defect density. After spectral integration over the ZPL width, we get a ratio of around 3:1 for the "4 eV defect" emission intensity in hBN and bBN, taking into account the two defect configurations in the AB stacking that are almost equiprobable in the investigated bBN crystal of Fig.2**, as seen in Fig.4(b-c) in the Appendix**. Whatever the intrinsic or extrinsic nature of the "4 eV defect" (still highly debated [14–28]), this 3:1 ratio indicates an almost identical defect density in the hBN and bBN crystals, suggesting a comparable efficiency of the defect creation in the AA' and AB stackings.

Hyperspectral imaging in the UV-C shows that the AB stacking can exist in a micro-crystal but also at the edges of a hBN crystal in the AA' stacking [Fig.1(b)]. Despite the fact that the noncentrosymmetric AB stacking is marginal at the edges of the hBN crystal, the modification of the "4 eV defect" emission at these edges is the same as in the bBN crystal, with an identical 50 or 70 meV blueshift of the ZPL accompanied by a 2 meV broadening. The correlation of the PL maps detected in the UV-C and UV-B ranges [Fig.1(b) and Fig.2(b)] illustrates that ZPLs at 4.14 or 4.16 eV are specific to the noncentrosymmetric AB stacking, and it further demonstrates the dependence of the "4 eV defect" emission with the stacking sequence.

The stacking-dependent correspondence of the optical response between the UV-C and UV-B ranges being established, we highlight the relevance of studying the "4 eV defect" emission in the context of polytypism in boron nitride. The identification of different sp^2-bonded boron nitride polytypes is difficult. It remains very challenging and a key issue in the context of the epitaxial growth of boron nitride layers and their characterization by X-ray diffraction [35]. Our recent identification of bBN crystals by hyperspectral cryomicroscopy in the UV-C shines a new light on this topic by providing specific informations on the AB stacking. Still, optical spectroscopy in the UV-C is far from a routine method, and our present results open a way for an easier investigation of polytypism in sp^2-bonded boron nitride by careful inspection of the "4 eV defect" emission, in the UV-B range. The PL of this deep level can be excited by the third-harmonic of a Ti:Sa laser and by standard 266 nm-lasers based on nonlinear generation from a YAG laser. Furthermore, detection of the PL signal at ∼300 nm is simpler than at ∼200 nm because optical spectroscopy in the UV-B is much less constrained than in the UV-C. We expect the "4 eV defect" emission to become a probe of the stacking order in sp^2-bonded boron nitride polytypes.

From another perspective, our results should fuel theoretical investigations by pointing out the importance of considering the stacking sequence in *ab initio* calculations. Many microscopic structures have been proposed for the "4 eV defect" [24–28], and our data show that the stacking order is an important degree of freedom to consider. Calculations shall not only go beyond boron nitride monolayers and be implemented in bulk, but they

should also explore various stacking sequences in order to identify the configurations that are compatible with the stacking dependence of the ZPL energy, and to possibly elucidate the defect structure. Furthermore, the influence of polytypism on the electronic states of defects may be important in the context of understanding and controlling the doping of boron nitride.

IV. CONCLUSION

We have studied sp^2-bonded boron nitride polytypes by hyperspectral cryomicroscopy in the UV-C and UV-B spectral ranges. By comparing two different polytypes extracted from the same polycrystalline sample, we have revealed that the "4 eV defect" emits at different energies depending on the polytype. There are two possible defect configurations in the AB stacking, with a ZPL blue-shift of 50 and 70 meV with respect to the AA' stacking. Our results open the way for novel characterization methods of the stacking order in sp^2-bonded boron nitride, and bring novel inputs for the elucidation of the atomistic configuration of points defects by advanced *ab initio* calculations.

Acknowledgments We gratefully acknowledge C. L'Henoret and T. Cohen for their technical support at the mechanics workshop. This work was financially supported by the network GaNeX (ANR-11-LABX-0014) and the BONASPES project (ANR-19-CE30-0007). JL and JHE are grateful for support from the Office of Naval Research, award number N00014-20-1-2474, for the BN crystal growth.

*e-mail: guillaume.cassabois@umontpellier.fr

V. APPENDIX

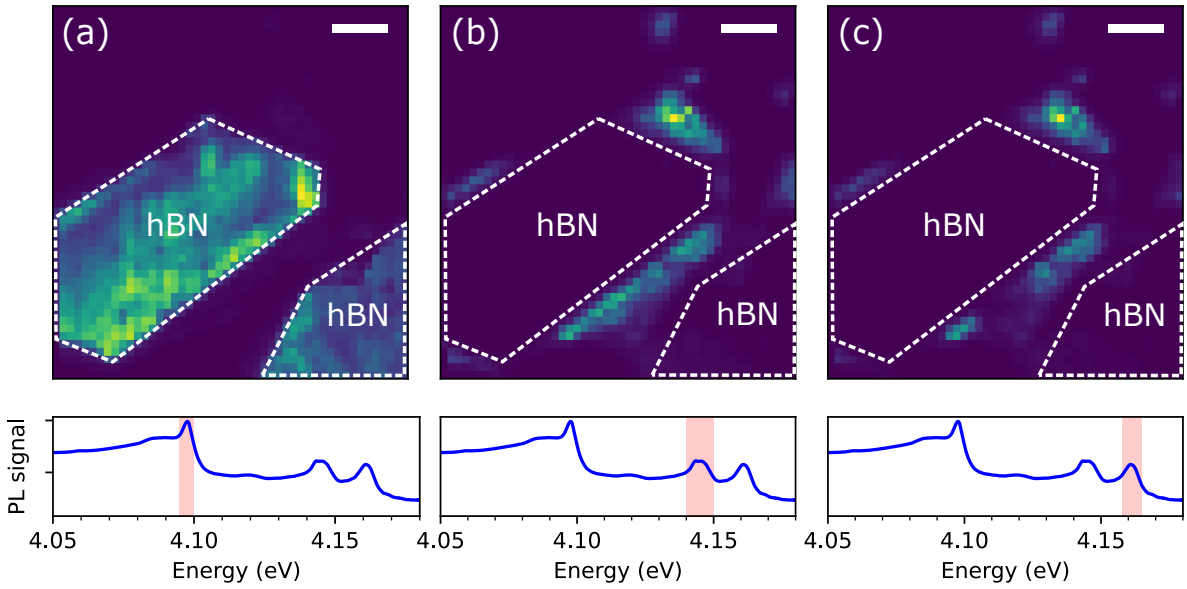

FIG. 4. Maps of the PL signal in the spectral domain indicated by the shaded area in the PL spectra plotted below: (a) around ∼4.09 eV, (b) around ∼4.14 eV, and (c) around ∼4.16 eV. Dashed lines are guides for the eyes. Scale bar = 4 μm.

[1] A. Tararan, S. di Sabatino, M. Gatti, T. Taniguchi, K. Watanabe, L. Reining, L. H. G. Tizei, M. Kociak, and A. Zobelli, Phys. Rev. B **98**, 094106 (2018).

[2] J. Y. Tsao, S. Chowdhury, M. A. Hollis, D. Jena, N. M. Johnson, K. A. Jones, R. J. Kaplar, S. Rajan, C. G. Van de Walle, E. Bellotti *et al.*, Adv. Electron. Mater. **4**, 1600501 (2018).

[3] R. S. Pease, Acta Cryst. **5**, 356 (1952).

[4] K. Watanabe, T. Taniguchi, and H. Kanda, Nat. Mater. **3**, 404 (2004).

[5] A. K. Geim and I. V. Grigorieva, Nature **499**, 419 (2013).

[6] K. Watanabe, T. Taniguchi, T. Niiyama, K. Miya, and M. Taniguchi, Nat. Photon. **3**, 591 (2009).

[7] J. Caldwell, I. Aharonovich, G. Cassabois, J. H. Edgar, B. Gil, and D. N. Basov, Nat. Rev. Mat. **4**, 552 (2019).

[8] B. Gil, G. Cassabois, R. Cuscó, G. Fugallo and L. Artús, Nanophotonics, Vol. **9**, 3483 (2020).

[9] G. Cassabois, P. Valvin, and B. Gil, Nat. Photon. **10**, 262 (2016).

[10] R. Schuster, C. Habenicht, M. Ahmad, M. Knupfer, and B. Büchner, Phys. Rev. B **97**, 041201 (2018).

[11] B. Gil, W. Desrat, A. Rousseau, C. Elias, P. Valvin, M. Moret, J. Li, E. Janzen, J. H. Edgar, and G. Cassabois, Crystals **12**, 782 (2022).

[12] A. Rousseau, P. Valvin, W. Desrat, L. Xue, J. Li, J. H. Edgar, G. Cassabois, and B. Gil, ACS Nano **16**, 2756 (2022).

[13] A. Rousseau, M. Moret, P. Valvin, W. Desrat, J. Li, E. Janzen, L. Xue, J. H. Edgar, G. Cassabois, and B. Gil, Phys. Rev. Mat. **5**, 064602 (2021).

[14] A. Katzir, J. T. Suss, A. Zunger, and A. Halperin, Phys. Rev. B **11**, 2370 (1975).

[15] T. Kuzuba, K. Era, T. Ishii, T. Sato, and M. Iwata, PhysicaA&B **105**, 339 (1981).

[16] T. Taniguchi and K. Watanabe, J. Cryst. Growth **303**, 525 (2007).

[17] L. Museur, E. Feldbach, and A. Kanaev, Phys. Rev. B **78**, 155204 (2008).

[18] T.Q.P. Vuong, G. Cassabois, P. Valvin, A. Ouerghi, Y. Chassagneux, C. Voisin, and B. Gil, Phys. Rev. Lett **117**, 097402 (2016).

[19] E. Tsushima, T. Tsujimura, and T. Uchino, Appl. Phys. Lett. **113**, 031903 (2018).

[20] S. Chichibu, Y. Ishikawa, H. Kominami and K. Hara, J. Appl. Phys. **123**, 065104 (2018).

[21] A. Vokhmintsev, I. Weinstein, and D. Zamyatin, J. Lumin. **208**, 363 (2019).

[22] A. S. Vokhmintsev, I. A. Weinstein, M. G. Minin, and S. A. Shalyakin, Radiat. Meas. **124**, 35 (2019).

[23] T. Pelini, C. Elias, R. Page, L. Xue, S. Liu, J. Li, J. H. Edgar, A. Dréau, V. Jacques, P. Valvin, B. Gil, and G. Cassabois, Phys. Rev. Mat. **3**, 094001 (2019).

[24] C. Attaccalite, M. Bockstedte, A. Marini, A. Rubio, and L. Wirtz, Phys. Rev. B **83**, 144115 (2011).

[25] L. Weston, D. Wickramaratne, M. Mackoit, A. Alkauskas, and C. G. Van de Walle, Phys. Rev. B **97**, 214104 (2018).

[26] T. Korona and M. Chojecki, Int. J. Quantum Chem. **119**, e25925 (2019).

[27] M. Mackoit-Sinkevičienė, M. Maciaszek, C. Van de Walle, and A. Alkauskas, Appl. Phys. Lett. **115**, 212101 (2019).

[28] S. Li, A. Pershin, G. Thiering, P. Udvarhelyi, and A. Gali, J. Phys. Chem. Lett. **13**, 3150 (2022).

[29] L. Sponza, H. Amara, C. Attaccalite, S. Latil, T. Galvani, F. Paleari, L. Wirtz, and F. Ducastelle, Phys. Rev. B **98**, 125206 (2018).

[30] K. A. Mengle and E. Kioupakis, APL Materials **7**, 021106 (2019).

[31] S. M. Gilbert, T. Pham, M. Dogan, S. Oh, B. Shevitski, G. Schumm, S. Liu, P. Ercius, S. Aloni, M. L. Cohen, and A. Zettl, 2D Mater. **6**, 021006 (2019).

[32] C. Elias, G. Fugallo, P. Valvin, C. L'Henoret, J. Li, J. H. Edgar, F. Sottile, M. Lazzeri, A. Ouerghi, B. Gil, G. Cassabois, Phys. Rev. Lett. **127**, 13, 137401 (2021).

[33] P. Valvin, T. Pelini, G. Cassabois, A. Zobelli, J. Li, J. H. Edgar, and B. Gil, AIP Advances **10**, 075025 (2020).

[34] A. Rousseau, L. Ren, A. Durand, P. Valvin, B. Gil, K. Watanabe, T. Taniguchi, B. Urbaszek, X. Marie, C. Robert, and G. Cassabois, Nano Lett. **21**, 10133 (2021).

[35] M. Moret, A. Rousseau, P. Valvin, S. Sharma, L. Souqui, H. Pedersen, H. Högberg, G. Cassabois, J. Li, J. H. Edgar, and B. Gil, Appl. Phys. Lett. **119**, 262102 (2021).